Neutral-Boson Photoproduction on Hydrogen at High Energies*

R. Anderson, D. Gustavson, J. Johnson, D. Ritson, and B. H. Wiik

Stanford Linear Accelerator Center, Stanford University, Stanford, California 94305

AND

W. G. Jones† and D. Kreinick

California Institute of Technology, Pasadena, California 91109

AND

F. Murphy

University of California, Santa Barbara, California

AND

R. Weinstein

Northeastern University, Boston, Massachusetts 02115

(Received 15 September 1969)

Photoproduction cross sections for neutral π, η, ρ, and ϕ mesons have been measured at the Stanford Linear Accelerator Center for photon energies between 5 and 17.8 GeV, and t (four-momentum transfer squared) between -0.12 and -1.4 $(\text{GeV}/c)^2$, using a missing-mass technique. The pion production at lower energies is characterized by a fast falloff with increasing $|t|$ at small $|t|$ values, with a dip at $t = -0.5$ $(\text{GeV}/c)^2$ followed by a secondary maximum around $t = -0.9$ $(\text{GeV}/c)^2$ and a smooth falloff at larger $|t|$ values. As the incident photon energy increases, the dip becomes less pronounced, in contradiction to the expectations of simple Regge theories based only on the exchange of the ω and B trajectories. η photoproduction was measured around 6 GeV and at 9 GeV. The cross section decreases smoothly with t and shows no dip at $t = -0.5$ $(\text{GeV}/c)^2$, in disagreement with predictions based on Reggeized ρ exchange. ρ production rates agree well with predictions assuming diffraction production. The differential cross section varies approximately as $e^{8.5t}$. The total cross section decreases from 16.0 μb at 5.5 GeV to 12.3 μb at 17.8 GeV incident photon energy. A quark-model relation between π-p elastic scattering and ρ photoproduction gives a good representation of the data. ϕ production also appears consistent with the predictions of the diffraction-dissociation model. We also searched for evidence of photoproduction of other particles with mass up to 2 GeV. Production of one particle of mass 1240±20 MeV and width around 100 MeV was observed. No particles with mass between 1300 and 2000 MeV were found. Any particle with cross section larger than 4% of the ρ cross section would have been visible.

I. INTRODUCTION

IN this experiment we have extended previous data on neutral meson photoproduction cross sections to higher energies and a broader range of four-momentum transfers. The experiment was carried out at the Stanford Linear Accelerator Center (SLAC) using the SLAC 1.6-GeV/c spectrometer as a missing-mass spectrometer. Some preliminary results of this experiment have already been published.[1]

Earlier measurements have been made on forward neutral pion photoproduction by groups at DESY,[2] and at CEA[3] in the photon energy range 2–5.8 GeV. Their results showed a pronounced dip in the cross sections at a value of the four-momentum transfer squared $t = -0.5$ $(\text{GeV}/c)^2$. There has been considerable speculation on what the form of the energy dependence for this process would be at higher energies.[4,5] The

earlier data could be understood within the framework of a conventional Regge theory by assuming ω and B exchange.[5] This theory predicted that the B-meson exchange would become less important at higher energies and that the process would eventually be completely dominated by ω exchange. Assuming that the ρ and ω trajectories were similar, it was then expected that the neutral pion photoproduction cross section would be similar to the $\pi^- + p \rightarrow \pi^0 + n$ charge-exchange cross section, where only ρ exchange is permitted, i.e., that the cross section for neutral pion photoproduction would show both a shrinking of the forward peak with increasing energy and a sharp dip at $t = -0.5$ $(\text{GeV}/c)^2$. Our data extend to photon energies of 15 GeV and appear to be in disagreement with these predictions.

We have also measured η photoproduction around 6 GeV and at 9 GeV. Lower-energy data[6] covering a similar range in t exist from experiments at the CEA. The results are mainly interesting for their behavior near $t = -0.5$ $(\text{GeV}/c)^2$. In conventional Regge theory, the process is expected to have a large contribution from

[1] R. Anderson *et al.*, Phys. Rev. Letters **21**, 384 (1968); W. G. Jones *et al.*, *ibid.* **21**, 586 (1968).
[2] M. Braunschweig *et al.*, Phys. Letters **26 B**, 405 (1968).
[3] G. C. Bolon *et al.*, Phys. Rev. Letters **18**, 926 (1967).
[4] M. P. Locher and H. Rollnik, Phys. Letters **22**, 696 (1966).
[5] J. P. Ader, M. Capdeville, and Ph. Salin, Nucl. Phys. **B3**, 407 (1967).

[6] D. Bellenger *et al.*, Phys. Rev. Letters **21**, 1205 (1968).

ρ-meson exchange and, therefore, it should show a sharp dip at $t=-0.5$ $(\text{GeV}/c)^2$. No such dip is observed.

Our measurements of neutral ρ photoproduction extend to higher energies than previous data.[7-10] The results of these experiments at lower energies have been successfully explained in the framework of the vector-meson-dominance theory. According to this theory, the cross section for photoproduction of a vector meson V^0 should be proportional at higher energies to the cross section for the elastic scattering of transversely polarized vector mesons from hydrogen, i.e.,

$$\frac{d\sigma}{dt}(\gamma+p \to V^0+p)$$
$$=\tfrac{1}{4}\alpha\frac{4\pi}{\gamma_V{}^2}\frac{d\sigma}{dt}(V^0{}_{\text{tr}}+p \to V^0{}_{\text{tr}}+p), \quad (1.1)$$

where $\alpha=1/137$, and γ_V describes the coupling of a virtual vector meson to a real photon. On the basis of a broken-$SU(3)$ quark model,[11] the cross section for the elastic scattering process $\rho^0+p \to \rho^0+p$ is given by

$$\frac{d\sigma}{dt}(\rho^0 p)=\left[\frac{1}{2}\left(\frac{d\sigma}{dt}(\pi^+ p)\right)^{1/2}+\frac{1}{2}\left(\frac{d\sigma}{dt}(\pi^- p)\right)^{1/2}\right]^2. \quad (1.2)$$

These relations are well satisfied for neutral ρ photoproduction over the whole kinematic range covered in this experiment.

Previous to this experiment, few experimental data were available on the photoproduction of the ϕ meson.[8,12] ϕ production, though small, should be largely diffractive. The results of this experiment in the energy range 6–18 GeV support this assertion. The t dependence of the cross section is again reproduced with a broken-$SU(3)$ quark-model prediction.[11,13]

No previous firm observations[14] have been made on the photoproduction of higher-mass mesons at high energies. We observed the production of a meson in the mass region around 1240 MeV, tentatively identified with the B meson. We searched for vector-meson production in the region of masses 1.3–2 GeV, and might have expected to observe the $J^{PC}=1^{--}$ "daughter"

to the ρ meson around 1500 MeV. No such meson was found.

II. EXPERIMENT AND APPARATUS

A. Experimental Arrangement

The experiment was carried out at the Stanford Linear Accelerator Center. The layout of the experiment is shown in Fig. 1. The momentum-analyzed electron beam was focused onto an aluminum radiator, 0.03 radiation lengths thick, located about 150 ft upstream of the target. A sweeping magnet, placed just after the radiator, deflected the main electron beam into a beam dump. The photon beam was then collimated to the required size by a high-power water-cooled collimator (C-10) before impinging on the liquid-hydrogen target. Secondary collimators were set up to intercept any halo of the beam remaining after the collimation by C-10. There were also several sweep magnets in the beam line to remove electron spray produced by these collimators. The photon beam finally stopped in a secondary-emission quantameter (SEQ) located approximately 100 ft downstream from the target. This SEQ was our primary beam monitor. In addition, the beam intensity was monitored by a Čerenkov monitor as well as a secondary emission monitor (SEM), both located in the front of the target as indicated in Fig. 1. The intensity of the photon beam incident on the target was typically 5×10^{11} equivalent quanta per second.

The target used was of a condensation type.[15] The target cell was a cylinder, 15 in. long and 2 in. in diameter, made out of 0.008-in.-thick Mylar with thin aluminum end caps. A "dummy cell" and a "no cell" position were also available.

B. Spectrometer and Counter System

The SLAC 1.6-GeV/c spectrometer[16] was used to analyze the recoiling protons. It is a weak-focusing $(n=0)$, second-order-corrected, 90° vertical bend magnet with a radius of 100 in. The momentum acceptance and the acceptance in production angle are defined by the size of the counters in the focal plane. The azimuthal angle $(\Delta\varphi)$ and the useful target length were determined by remotely movable slit systems placed at the spectrometer entrance. For this experiment the total acceptance was $(\Delta p/p)\Delta\Omega=6.8\times10^{-5}$ sr and the useful target length was typically about 7 in.

The spectrometer focused production angles and momenta onto a single focal plane which was normal to the direction of the focused particles and had a linear dispersion of 1.66 in./% in momentum and 0.32 in./mrad in angle. The resolution was $\pm0.08\%$ in momentum and ±0.4 mrad in angle. The locus of particles from a particular two-body reaction can be approximated by a straight line over the small momentum and angle

[7] F. M. Pipkin, in *Proceedings of the Third International Symposium on Electron and Photon Interactions at High Energies, Stanford Linear Accelerator Center, 1967* (Clearing House of Federal Scientific and Technical Information, Washington, D. C., 1968).

[8] S. C. C. Ting, in *Proceedings of the Fourteenth International Conference on High-Energy Physics, Vienna, 1968* (CERN, Geneva, 1968), p. 43.

[9] G. McClellan *et al.*, Phys. Rev. Letters **22**, 374 (1969).

[10] M. Davier *et al.*, Phys. Rev. Letters **21**, 841 (1968).

[11] H. J. Lipkin, Phys. Rev. Letters **16**, 1015 (1966); H. Joos, Phys. Letters **24B**, 103 (1967); M. Davier, Phys. Rev. Letters **20**, 952 (1968). The model was extended to finite values of t by B. Margolis, Nucl. Phys. **B6**, 687 (1968).

[12] DESY Bubble Chamber Collaboration, Phys. Rev. **175**, 1669 (1968); M. Davier *et al.*, Phys. Rev. Letters **28B**, 619 (1969).

[13] K. Kajantie and J. S. Trefil, Phys. Letters **24B**, 106 (1968).

[14] E. Lohrmann, in *Proceedings of the Third International Symposium on Electron and Photon Interactions, Stanford Linear Accelerator Center, 1967* (Clearing House of Federal Scientific and Technical Information, Washington, D. C., 1968).

[15] R. L. Anderson, Nucl. Instr. Methods **70**, 87 (1969).

[16] R. L. Anderson *et al.*, Nucl. Instr. Methods **66**, 328 (1968).

acceptance of the spectrometer focal plane. Hence a two-body process can be selectively detected by a hodoscope counter aligned along the appropriate kinematic curve. This technique eliminated complex decoding and made it possible to record several events during the 1.6-μsec-long SLAC beam pulses with simple electronics.

The momentum calibration and the solid angle had been previously determined both by a wirefloat measurement and by running a well-defined electron beam from the accelerator directly into the spectrometer. The estimated error was $\pm0.2\%$ in the momentum calibration and $\pm3\%$ in the total acceptance $(\Delta p/p)\Delta\Omega$. We estimate that the uncertainty in the determination of the production angle with respect to the direction of the photon beam was ±0.3 mrad.

The spectrometer and the counter system are shown in Fig. 2; the counter system is shown in more detail in the insert. The telescope consists of five scintillation counters (S9–S13) made out of Pilot B plastic; S9 and S10 were $7\times11\times0.5$ in. and S11–S13 were $10\times14\times0.5$ in. Between S10 and S11 and between S11 and S12 there were remotely variable absorber changers. A missing-mass hodoscope consisting of eight elements, each $0.75\times10\times0.25$ in., was located between S9 and S10. For counters S9 and S10, Amperex XP1020 photomultiplier tubes were used; for all other scintillation counters, RCA 7850's were used. A threshold Lucite Čerenkov counter ($9\times13\times2$ in.) was inserted between S10 and S11. The counter was so constructed that only light which was internally reflected could reach the phototubes. The outputs of the four RCA 8575 photomultiplier tubes used to view the Lucite were added linearly. The counter was 98% efficient for pions and counted protons with less than 2% efficiency below 1000 MeV/c, increasing to 6% at 1400 MeV/c. The whole counter system was remotely rotatable so that the hodoscope counters could be aligned along lines of constant missing mass in the focal plane.

For low t values $[|t|<0.4$ (GeV/c)$^2]$, the protons were identified by range and pulse height using the first few trigger counters. At higher $|t|$ values, the threshold Čerenkov counter was used in veto to provide additional rejection against pions. The ratio of the pion flux to the proton flux incident on the counters was typically 1:1 near the π^0 threshold and the above criteria reduced the pion contamination to the 1% level. The last two scintillation counters, S12 and S13, had their biases set low and were put in coincidence with the threshold Čerenkov counter to monitor the flux of produced π^+ mesons.

To measure the efficiencies of the system for protons and pions we used the chopped SLAC electron beam and a time-of-flight system.[17] This provided us with a clean separation of protons and pions and allowed the

---

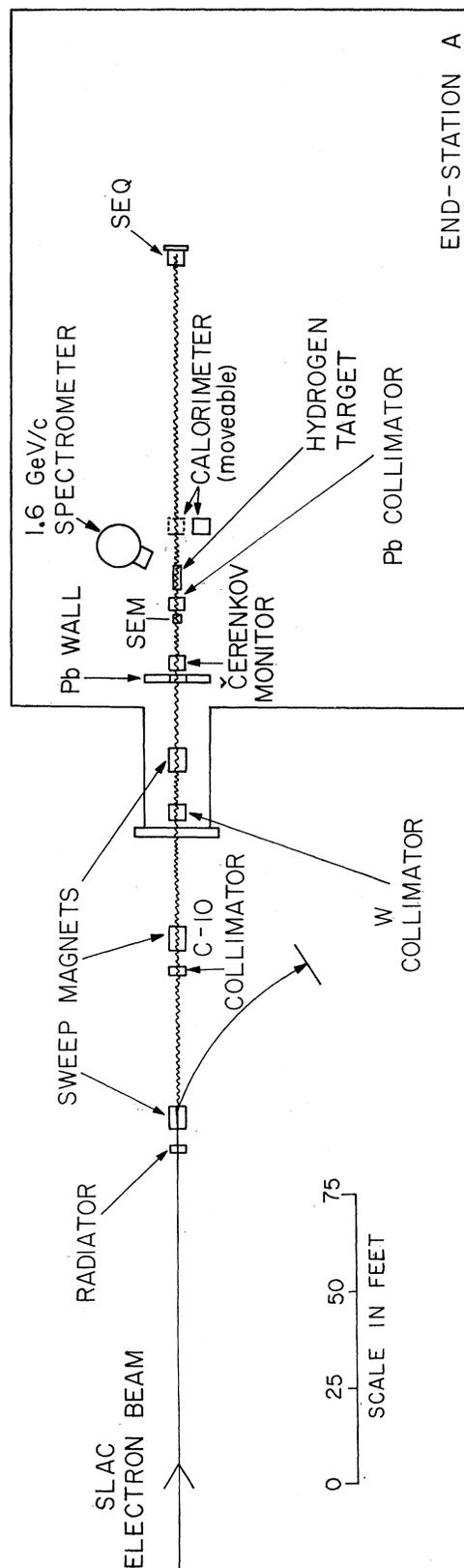[17] R. L. Anderson and D. Porat, Nucl. Instr. Methods **70**, 77 (1969).
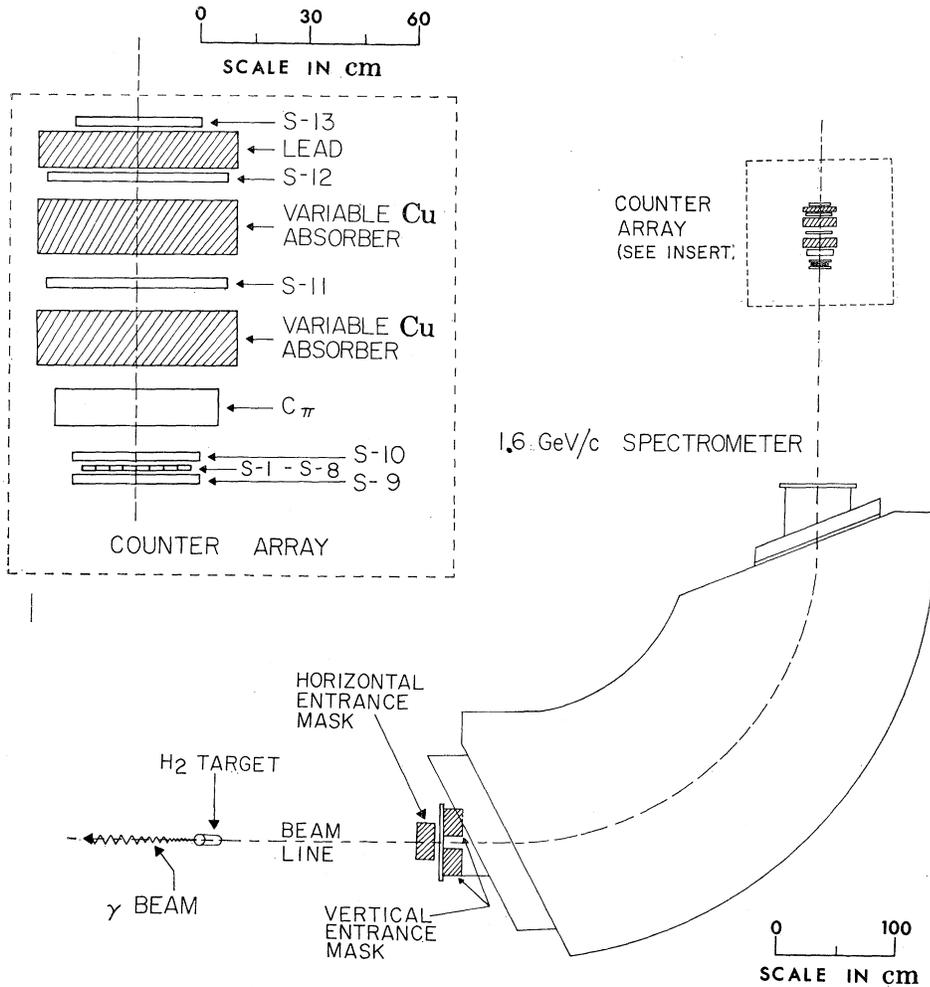

FIG. 1. Experimental arrangement.

FIG. 2. Positioning of the spectrometer and the counters relative to the beam line and the target. The insert shows the detector system in more detail.

detection efficiencies of the system to be determined. The efficiencies of the individual hodoscope elements were determined for each run and were near 100%.

C. Electronics

Figure 3 shows a simplified block diagram of the electronics. Standard 100-Mc modules[18] were used for the logic. The event rate was quite high, up to six counts in the 1.6-μsec-long beam pulse. The interesting rates were therefore all fed into fast 100-Mc scalers[19] and stored there for the duration of an experimental run. After each run, the scalers and other relevant data were read by the SLAC SDS-9300 computer.

D. Beam Monitors

The primary beam monitor was a nonsaturating quantameter.[20] The quantameter was fully evacuated and consisted of 20 copper plates 0.5 in. thick alternated with 19 foils of gold-plated aluminum each 0.0005 in. thick. The device was calibrated against the SLAC silver calorimeter[21] as well as against a Faraday cup. The average calibration constant was 2.92 electrons/ GeV for a voltage of $+750$ V. The absolute calibrations were repeated periodically during the course of the experiment and were found reproducible within 1%. However, we assigned an over-all error of $\pm2\%$ to our absolute calibration value.

The relative stability of our monitor systems, when conditions were carefully standardized, was $\pm0.2\%$. We used the SLAC photon-beam Čerenkov monitor[21] for an additional check. This consisted of a tube 30 in. long filled with He gas at about 1 atm. The light was focused onto a photomultiplier tube, whose output was then integrated. The ratio of the Čerenkov monitor to the SEQ remained constant to fractions of a percent for periods of hours.

[18] Chronetics, Inc., Mount Vernon, N. Y.

[19] Transistor Specialities Incorporated, Terminal Drive, Plainview, L. I., N. Y.

[20] R. L. Anderson, Nucl. Instr. Methods **65**, 195 (1968).

[21] G. Fisher and Y. Murata, SLAC Report No. SLAC-PUB-605, 1969 (unpublished).

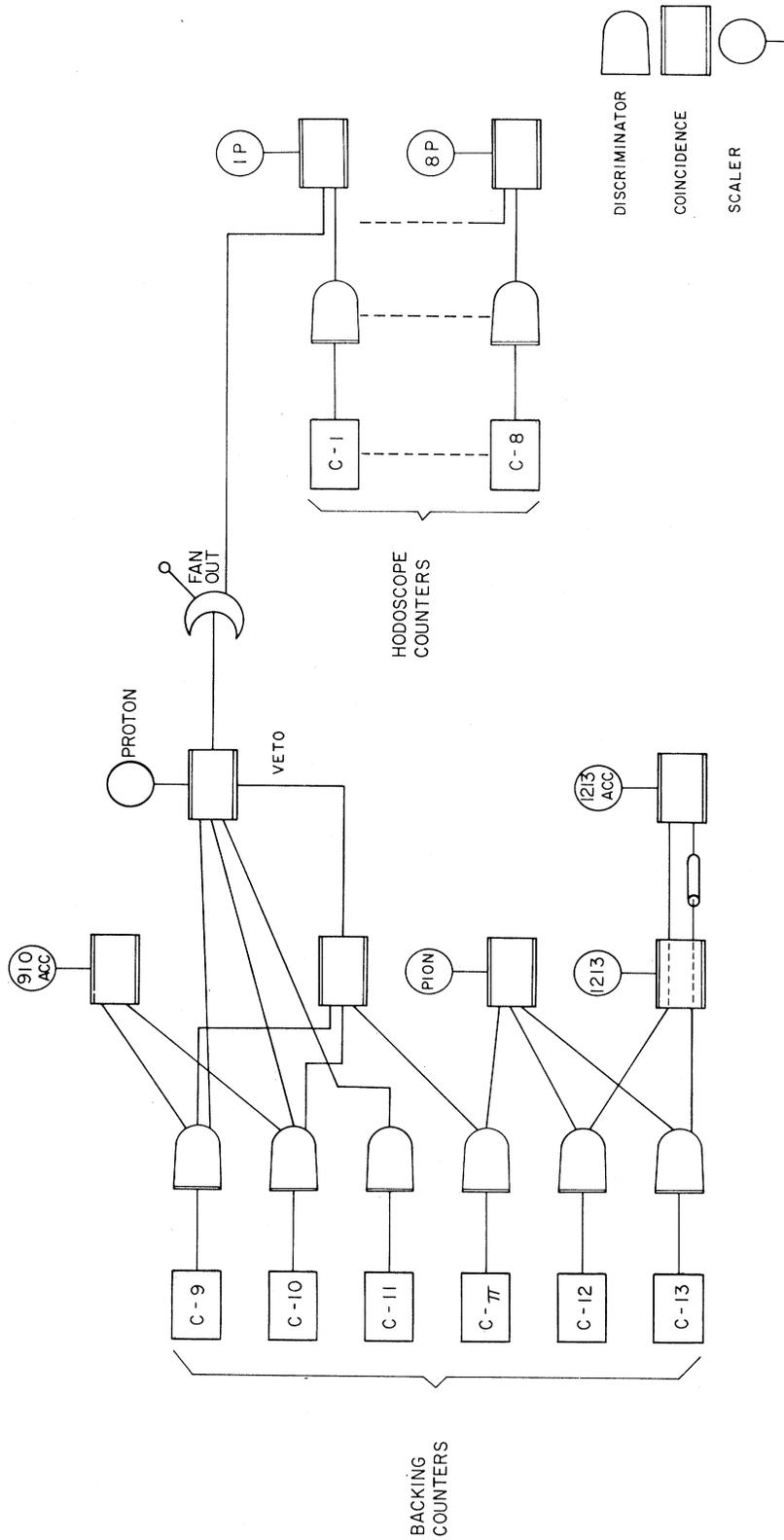FIG. 3. Block diagram of the electronics. Only the main logic is shown.

E. Data Accumulation and Reduction

The choice of the hodoscope angle determined the angular production width $\Delta\theta$ accepted by one hodoscope counter and the range of angles was then divided into bins, each $\Delta\theta$ wide. This bin width was typically about 2.8 mrad. To reduce our sensitivity to small drifts in the apparatus, the data were accumulated in an interlaced pattern over the angular range of interest and each angular point or bin was measured on several and in many cases on all eight hodoscope counters. Since the π^+-meson yield curve, measured simultaneously by a coincidence between counters S12, S13, and the threshold Čerenkov counter, should vary smoothly with angle in this kinematic region, a valuable additional cross-check on the beam and monitor stability was available.

Each run at a given angle lasted typically 5 min. After the run the relevant data were all read in, stored, and recorded on magnetic tape by the SLAC SDS-9300 computer. The hodoscope data were accumulated in bins and an automatic plotting machine plotted each run individually to aid the experimenter in checking for consistency. The accumulated data could be plotted on demand and selected runs on the data tape could be added to or removed from the accumulation at any time.

Frequently the counting rate was measured as a function of beam intensity. This rate check was done by remotely varying the size of the photon collimator, leaving the beam structure as well as the beam steering intact.

Occasionally, empty-target runs were made. The empty-target rates were negligibly small compared with the full-target rates.

Subsequent to this the following steps were taken:

(1) Some runs were edited or discarded because of procedural errors in data taking.

(2) Each run was corrected for dead-time losses and accidental coincidences using the measured rate dependence. This combined correction was always kept less than 5%.

(3) Most data points were repeated on several elements of the hodoscope array. Differences in counting efficiency among the hodoscope elements were accounted for before these data points were combined to obtain our final yield curves. Because of the large degree of internal repetition and redundancy, the data could be cross-checked for internal consistency, relative monitor drifts, etc.[22] In the vast majority of runs, the external and internal error assignments were in agreement. In a few cases a small monitor change was detected and was found to correlate with a small change in the independently detected π^+-meson rate. These few runs were corrected or eliminated.

(4) We combined all the corrected data at fixed $|t|$

---

[22] D. L. Kreinick, Ph.D. thesis, California Institute of Technology (unpublished).

values and end-point energies into yield curves as a function of the spectrometer angle.

F. Analysis of Yield Curves

The production of a resonance particle X^0 in the reaction $\gamma + p \rightarrow X^0 + p$ corresponds to a "step" in the detected recoil proton yield measured as a function of angle for a fixed photon end-point energy. This missing-mass technique is very powerful for avoiding the complexities of detecting rapidly decaying particles as well as for surveying for the production of all possible particles in the same experimental setup. To see how each produced resonance must correspond to a "step" in a yield curve, let us first consider a monochromatic photon beam with energy k. In this case the missing mass is uniquely given by

$$M_X{}^2 = 2k(p\cos\theta - T) - 2MT. \qquad (2.1)$$

Here, p and θ are the momentum and angle, M is the mass, and T is the kinetic energy of the recoiling protons. Hence, by measuring the three-momentum of the recoiling proton, the mass of the produced "particle" X^0 is determined. Figure 4 shows the laboratory momentum of the recoil protons plotted versus angle in the laboratory for a fixed photon energy of 11.5 GeV. It is clear from this figure that by varying the spectrometer angle and keeping the momentum fixed, we get separate peaks corresponding to the different mass particles. In reality we are dealing with a bremsstrahlung beam, but for a fixed end-point energy k_0 of the photon spectrum and a fixed recoil momentum of the proton, we can always define a limiting angle θ_0 such that $M_X{}^2 = 0$. This corresponds to Compton scattering on the proton. At larger angles there are no kinematically allowed protons. At all smaller angles, protons from the Compton process are kinematically allowed. As we now move towards smaller angles with the spectrometer,
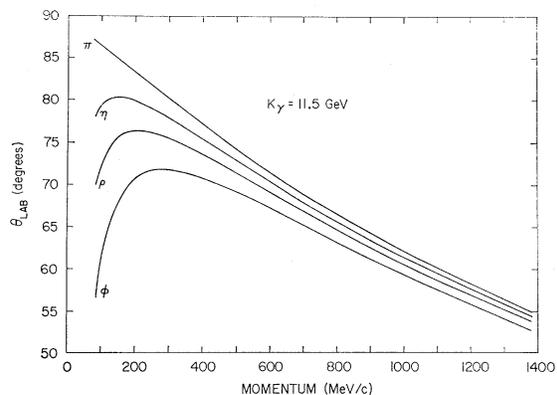
FIG. 4. Kinematics for photoproduction of various mesons for an incident photon energy of 11.5 GeV. Plotted is the momentum of the recoil proton versus its laboratory angle for π^0, η, ρ^0, and ϕ production. Note that for a fixed momentum the laboratory angle is nearly proportional to missing mass squared.

FIG. 5. (A) Measured proton yield for a peak bremsstrahlung energy of 11.5 GeV and for $t = -0.7$ (GeV/c)^2. The ordinate is the number of protons per hodoscope counter per 10^{11} E.Q. (equivalent quanta). The abscissa represents missing mass squared in GeV^2. The steps due to the onset of π^0, ρ^0, and ϕ production are clearly seen. The solid line through the data points represents a least-squares fit to the data assuming π^0, ρ^0, and ϕ production in addition to nonresonant background. The breakdown of the yield into the separate contributions is also shown. (B) Subtracted proton yield curve in counts per hodoscope counter per 10^{11} E.Q. for photons between 13.0 and 11.5 GeV and for $t = -0.7$ (GeV/c)^2. This curve was obtained by subtracting the 11.5-GeV proton yield from the corresponding proton yield at 13 GeV end-point energy. The peaks due to π^0, ρ^0, and ϕ production are again clearly seen. Because of multiple scattering of the recoil proton in traversing the target, the η is not clearly resolved from the ρ^0 peak. (C) Differential yield curve derived from the integral curve in (A). Plotted is the difference, in counts per 10^{11} E.Q., between once-removed yield points versus missing mass squared. Note the close similarity to the subtracted yield curve in (B).
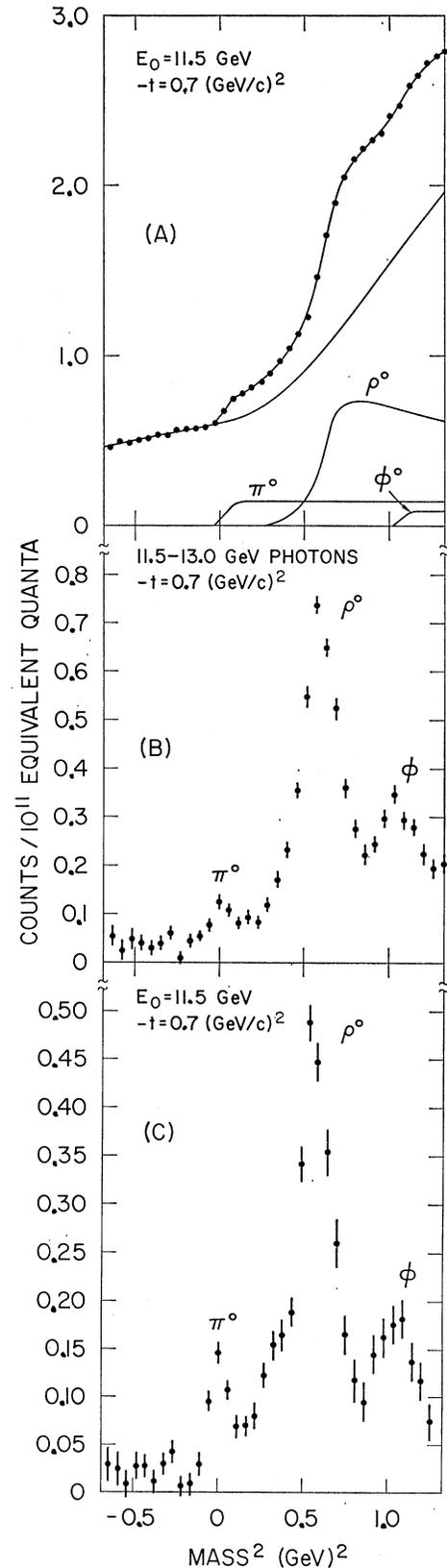
each new resonance will show up as a "step" on a rising yield curve.

Figure 5(A) shows such an experimentally measured yield curve for $k=11.5$ GeV and $t=-0.7$ $(GeV/c)^2$, and the breakdown of the yield into counts from the production of pions, ρ's, ϕ's, and nonresonant background. There was an appreciable yield of protons beyond the allowed kinematic limit because of the rescattering of forward-produced particles. This background was associated with the full target and was very small from the dummy target. As can be seen from Fig. 5(A), π^0 production showed up as a step on this "ghost proton" background. The angular resolution was not sufficient to separate the protons associated with π^0 production from those associated with Compton scattering, but at this particular angle and energy the Compton effect should be negligibly small compared with π^0 production. The shape of the leading edge of the pion step was almost completely determined by the angle changes due to multiple scattering of the recoil protons as they traversed the target. As the angle was decreased, recoil protons from successively higher masses were observed and the steps due to ρ and ϕ mesons can be clearly seen. A threshold missing-mass scale is provided for convenience, although in reality, photoproduction of all lower missing masses can produce recoil protons at the same angle and momentum. For example, at the angle in Fig. 5 corresponding to ϕ's made by 11.5-GeV photons, neutral ρ's are produced by 8.3-GeV photons, and neutral pions are produced by 4.8-GeV photons.

As a check on our procedures, yield curves were occasionally taken at closely adjacent energies E_1 and E_2. By subtracting the two yields with the appropriate corrections, a curve was obtained which corresponded to photoproduction by photons in the range E_1 to E_2. These subtracted curves showed the structure to be expected from a nearly "monochromatic" photon beam. Figure 5(B) shows such a curve obtained by subtracting the yields obtained with photon end-point energies of 13 and 11.5 GeV. Almost identical curves can be obtained by "differentiating" or taking successive differences of the yields on an integral yield curve obtained at one end-point energy. Figure 5(C) shows such a curve obtained by taking successive differences on the integral curve shown in Fig. 5(A). Note that the subtracted yield curve [Fig. 5(B)] and the first-difference curve [Fig. 5(C)] appear almost identical.

Cross sections were extracted by making a least-squares fit to a full sweep, fitting the positions and shapes of the various particles' yields, and assuming smooth backgrounds due to ghost protons and multi-particle production. The computer program accounted for kinematic factors, the correct bremsstrahlung spectra, resolution, and the variation of the cross section with energy. Subtracted yield curves, where available, were similarly fitted. The π^0, η, and φ steps were fitted also by eye, since the computer fits described above, although having the advantage of objectivity, suffer from inflexibility and the tendency of the large ρ^0 yield to dominate the solutions. The two approaches were considered to be complementary, and disagreements usually reflected genuine ambiguities in interpretation, which were accounted for in our quoted errors. Difficulties peculiar to each particle are discussed in the following sections; more detail is available in Ref. 22.

Our final cross sections include monitor calibrations, spectrometer calibrations, counter efficiencies, etc. Table I lists the various corrections, their magnitudes, and our estimates of the typical uncertainties in these corrections.

III. π^0 CROSS SECTIONS

Figure 6(A) shows a typical integral yield curve plotted against missing mass squared in the π^0 mass region. The sharp step due to the onset of the π^0 production is clearly seen. In the same figure the differential yield curve as derived from the integral curve is also shown. In this representation, π^0 production appears as a peak. The kinematic threshold for two-pion production is close to that for single-pion production. However, since two-pion production is a three-

TABLE I. Corrections and normalization uncertainties (in %).

Correction $\quad \diagdown -t \ (GeV/c)^2$	0.12	0.2	0.3	0.4	0.5	0.7	0.9	1.1	1.4
Acceptance correction[a] due to energy losses in target	18.7±1	7.5±0.4	3.3±0.2	1.9±0.1	1.4±0.1	0.7±0.1		negligible	
Proton losses (due to vetoing by C_π counter)		1 ±0.5	1 ±0.5	1 ±0.5	1 ±0.5	1 ±0.5	1.5±0.5	2.8±1.0	5.8±1.5
Hodoscope counter inefficiency	3 ±1	5 ±2	5 ±2	5 ±2	5 ±2	5 ±2	5 ±2	5 ±2	5 ±2
Nuclear absorption losses of protons	9 ±3	5 ±1	11 ±2	9 ±2	8 ±2	8 ±2	8 ±2	8 ±3	8 ±3
Solid-angle calibration of spectrometer	±3	±3	±3	±3	±3	±3	±3	±3	±3
Beam monitor[b] calibration	±2	±2	±2	±2	±2	±2	±2	±2	±2
Rate dependence				0–5%, with an uncertainty of ±2%					
Net over-all normalization uncertainty	5.3	4.8	5.0	5.0	5.0	5.0	5.0	5.5	5.7

[a] Spread in dP/P changes as a group of particles loses energy in traversing the target.
[b] Includes the uncertainty in the 3% correction for photons converted before reaching the target, and the estimated uncertainties in the calculated bremsstrahlung spectrum.

body process, it does not lead to a sharp step but rather to a smoothly rising yield curve starting at the threshold. This process was accounted for in the fitting programs by a polynomial starting at the two-pion threshold and including the experimental resolution. The difference between a three-body and a two-body process is sufficiently marked that we believe that this process is well accounted for in our cross-section determination and in our error assignments.
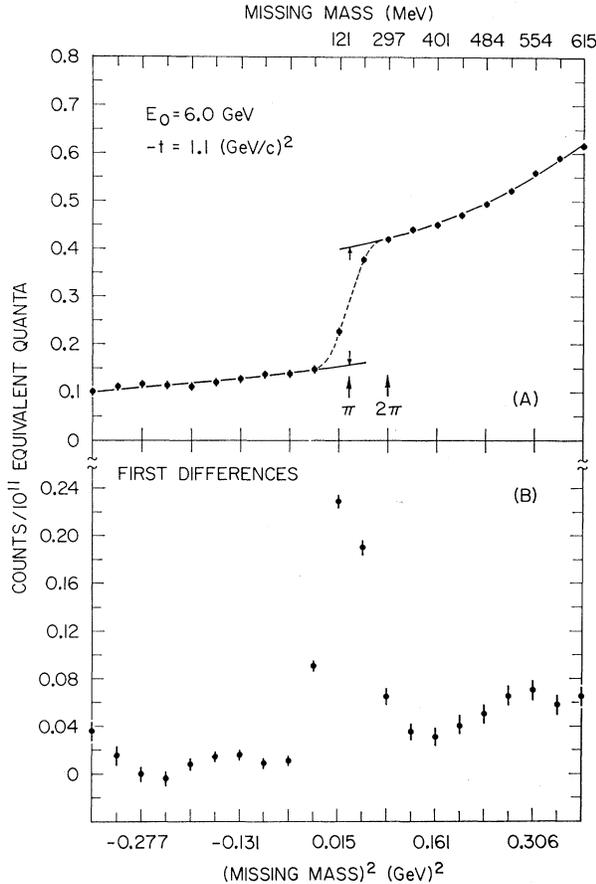

FIG. 6. (A) Measured proton yield in counts per hodoscope element per 10^{11} E.Q. plotted versus missing mass squared in the region around the π^0 step for a photon end-point energy of 6 GeV and for $t=-1.1$ $(\text{GeV}/c)^2$. (B) Differential yield curve derived from the integral yield in (A). Plotted is the difference, in counts per 10^{11} E.Q., between once-removed yield points versus missing mass squared.

Since the experimental resolution is not sufficient to separate π^0 production from Compton scattering, the cross sections extracted from the experimentally determined step heights must be reduced by the contribution of the Compton scattering. For this correction we assume the Compton cross section to be of the form $d\sigma/dt = Ae^{Bt}$, where $B=8.5$ $(\text{GeV}/c)^2$, e.g., the same slope as observed in the ρ^0 photoproduction on the proton. $A=0.68$ $\mu\text{b}/(\text{GeV}/c)^2$ was determined
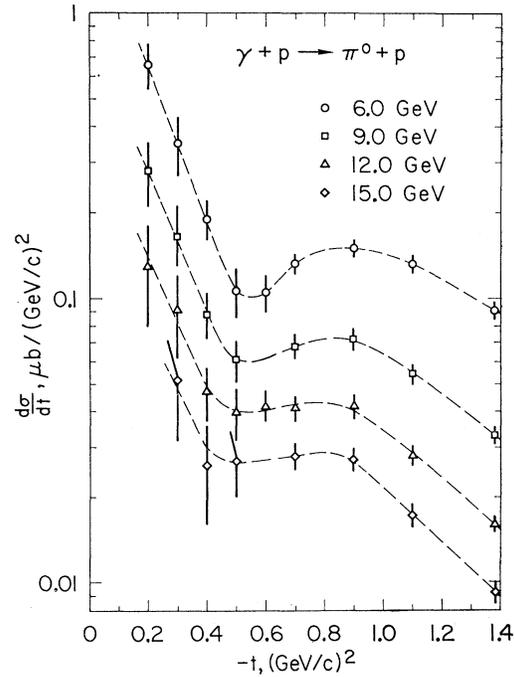

FIG. 7. $d\sigma/dt$ in $\mu\text{b}/(\text{GeV}/c)^2$ versus t for the reaction $\gamma+p \rightarrow \pi^0 +p$ at incident photon energies of 6, 9, 12, and 15 GeV. The lines drawn through the data are only to guide the eye.

from the total γ-p cross section using the optical theorem. The total γ-p cross section was set equal to 115 μb at high energies, in accordance with recent measurements.[23] The correction is important (50%) at low $|t|$ values and high energies. We estimate the correction to be known to $\pm 20\%$.

In Fig. 7, $d\sigma/dt$ determined from the step heights is plotted versus t for primary photon energies of 6, 9, 12, and 15 GeV. The data are characterized by a fast drop of the cross section at low $|t|$ values, a dip close to $t=-0.5$ $(\text{GeV}/c)^2$ followed by a secondary maximum at $t=-0.9$ $(\text{GeV}/c)^2$, and a smooth falloff with increasing $|t|$ values. With increasing photon energies the dip gradually becomes less pronounced.

Figure 8 shows our data at 6 GeV together with the DESY results[2] at 5 and 5.8 GeV for comparison. Plotted is $s^2\, d\sigma/dt$ versus t. The agreement is very satisfactory.

In Fig. 9, $d\sigma/dt$ versus $s-m^2$ is plotted for constant values of t. The DESY data[2] at lower energies are included in these plots. A least-squares fit to the data of the form $d\sigma/dt \sim (s-m^2)^{2\alpha-2}$ was made to the data at 3 GeV and above and is shown as the solid lines in Fig. 9. It clearly gives a very reasonable simultaneous representation of both our data and the DESY data. There is a small but significant amount of shrinkage with the effective Regge α, decreasing from $\alpha=0.16 \pm 0.05$ at $t=-0.7$ $(\text{GeV}/c)^2$ to $\alpha=-0.2\pm 0.05$ at
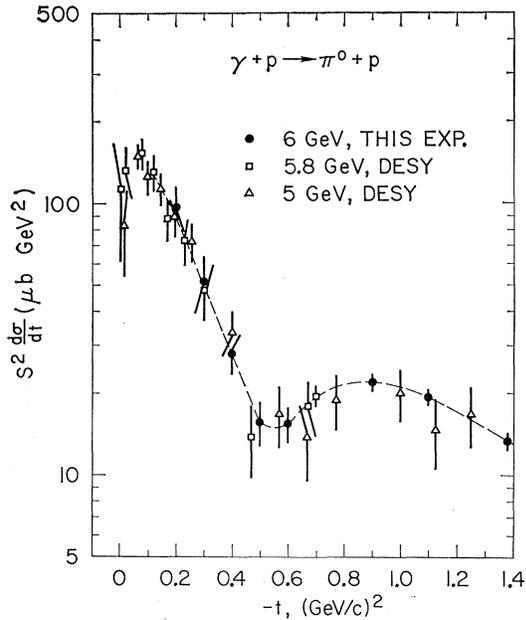
[23] D. Caldwell *et al.* (private communication).

FIG. 8. $s^2\, d\sigma/dt$ in μb GeV^2 plotted versus t for the reaction $\gamma+p \to \pi^0+p$. Plotted are the 6-GeV data together with data from DESY at 5 and 5.8 GeV. Data in the Primakoff region have been excluded.

$t=-1.4$ (GeV/c)^2. Below $|t|=0.5$ (GeV/c)^2, α remains close to 0. However, these points are more uncertain, since for low $|t|$ values and high energies the spread of photon energies corresponding to the width of the π^0 step becomes large. This spread arises from the angular uncertainty due to the multiple scattering of the recoil protons at small $|t|$ values combined with the kinematic factor $(dk/d\theta)_{\text{p=const}}$ which increases rapidly with decreasing $|t|$. The quoted errors on the low t points at high energies are largely systematic in origin and arise from our estimates of the above uncertainties. At high $|t|$ values, the resolution becomes entirely adequate and the quoted errors are mainly statistical.

The π^0 photoproduction at forward angles and high energies was originally expected[5] to be dominated by Reggeized particle exchange in the t channel. Charge-conjugation invariance requires the exchanged t-channel particle to be odd under C. Hence, of the established particles, only the neutral ρ, ω, ϕ, and B (or its isoscalar "relative" in the $J^P=1^+$ octet) need be considered. From a comparison of the coupling constants, one would expect ω exchange to dominate everywhere except in the vicinity of $t=-0.5$ (GeV/c)^2, where the ω trajectory goes through zero. This $|t|$ value corresponds to a supposed nonsense zero in the amplitude arising from ω exchange with a resulting dip in the cross section. Since the ω trajectory is very close to the ρ trajectory and ϕ exchange should be negligible, it was expected that in this dip region around -0.5 (GeV/c)^2 the cross section would be dominated by B exchange. At lower energies this picture agreed well with the

differential cross-section measurements at DESY and CEA.[2,3] This model further predicted that the dip in π^0 photoproduction would become more pronounced at higher energies and that the energy dependence of $d\sigma/dt$ would display strong shrinkage.

Neither of these predictions appears borne out by the results of this experiment. As we go to higher energies, the dip seems, if anything, to disappear and the shrinkage is much less than expected.[5] For instance, at $t=-0.9$ (GeV/c)^2, $d\sigma/dt\sim(s-m^2)^{-1.8}$, whereas from the accepted ω trajectory[24] we would expect $d\sigma/dt \sim (s-m^2)^{-3}$. That the cross section in the dip region is not dominated by B exchange (or the exchange of the isoscalar member of the "B octet") is also shown by measurements with polarized photons at 3 GeV.[25] These polarized-photon measurements have shown that the dominant exchange at these energies in the region of the dip has natural parity, thus excluding B exchange.

The combined experimental data on π^0 production, therefore, cannot be described in terms of simple Regge exchange. However, by including cuts or absorption in addition to the elementary Regge exchange, reasonably successful fits to the π^0 photoproduction data have been achieved.[26-29] The simplest cut term is the one that corresponds to the exchange of the Pomeranchukon P together with the ω. The effective trajectory $\alpha_C(t)$ can in this case be written as

$$\alpha_C(t)=\alpha_\omega(0)+\alpha_P(0)-1+\frac{\alpha_\omega{}'\alpha_P{}'}{\alpha_\omega{}'+\alpha_\omega{}'}\,t. \qquad (3.1)$$

Since this trajectory for physical $|t|$ values lies higher than the ω trajectory, we would expect the cut to dominate the cross section at sufficiently high energies.

Capella and Tran Thanh Van[26] attempt to fit the differential cross section as well as the polarized-photon data assuming only ω and ω-Pomeranchukon exchange. They achieve a good fit to the data using five free parameters. Contogouris and Lebrun[27] investigate the relationship between the pole terms and the cut terms, and compute the cut terms corresponding to ω exchange from a model. They achieve good fits to forward π^0 photoproduction as well as forward π^+ photoproduction using the same set of parameters.

Fröyland[28] introduces the ρ and ρ-Pomeranchukon cut in addition to the ω and ω-Pomeranchukon cut. He also achieves a good fit to the data, but this involves a large number of free parameters which are not uniquely determined from the experiment.

Blackmon, Kramer, and Schilling[29] try to fit the data

[24] G. Höhler *et al.*, Phys. Letters **20**, 79 (1966).

[25] D. Bellenger *et al.*, in *Proceedings of the Fourteenth International Conference on High-Energy Physics, Vienna, 1968* (CERN, Geneva, 1968).

[26] A. Capella and J. Tran Thanh Van, Nuovo Cimento Letters **1**, 321 (1969).

[27] A. P. Contogouris and J. P. Lebrun, Nuovo Cimento **64A**, 617 (1969).

[28] J. Fröyland, Nucl. Phys. **B11**, 204 (1969).

[29] M. L. Blackmon *et al.*, Phys. Rev. **183**, 1452 (1969).

FIG. 9. $d\sigma/dt$ in $\mu b/(GeV/c)^2$ for fixed t plotted versus $s-m^2$. Shown are the data from this experiment as well as data at lower energies from DESY. The solid line is a least-squares fit to the data of the form $d\sigma/dt\sim(s-m^2)^{2\alpha-2}$. The value of α is listed for each $|t|$ value.
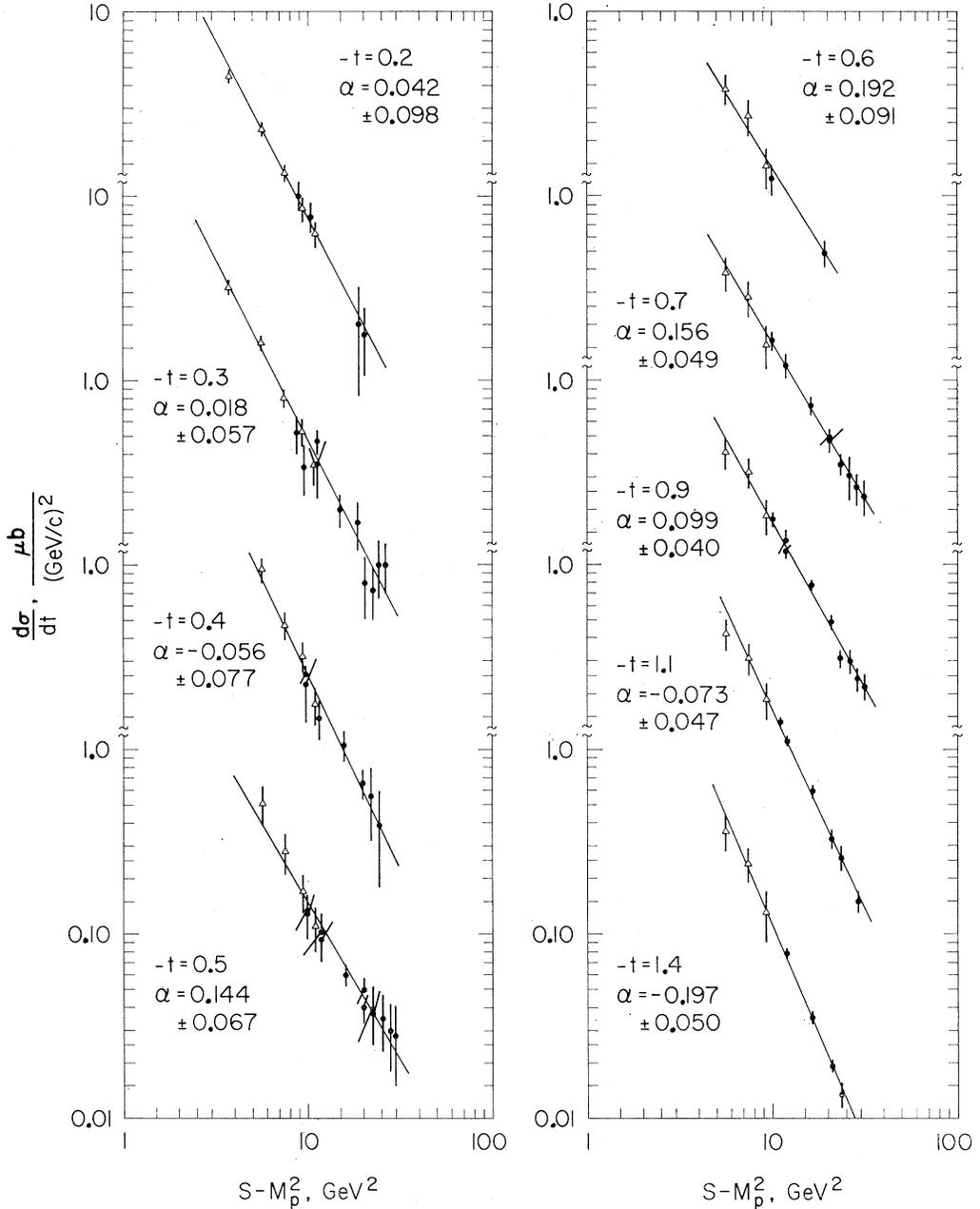
with ω and ρ exchange including absorption. They conclude they cannot get a good fit to the data with this model. They achieve a reasonable fit to all π^0 data by including B exchange in addition. However the B-meson trajectory $\alpha(t)=0.4+0.4t$, as determined from the fit, is much higher than expected and the slope is rather small.

It has been conjectured that a fixed pole at $J=0$

could be present in the π^0 photoproduction.[30] Such a pole would lead to an s^{-2} dependence of the cross section for sufficiently high energies in the region where α is negative. The present data seem to give no evidence for this.

[30] L. Jones, California Institute of Technology (private communication); for general discussion of fixed poles in photoproduction, see S. Mandelstam and L.-L. Wang, Phys. Rev. **160**, 1490 (1967).

Dar, Weisskopf, Levinson, and Lipkin[31] have compared the vector-dominance prediction of π^0 photoproduction with the experimental data. Unfortunately, the strong-interaction cross sections are not known at high energies and the low-energy measurements are not very accurate. Within the errors of the experiments, the vector-dominance-model prediction is well fulfilled at 6 GeV using $\gamma_\rho^2/4\pi = 0.5$.

IV. η PRODUCTION

Figure 10(A) shows an integral yield curve in the region of the η mass, at a primary photon energy of 5.5 GeV and $t = -0.5$ (GeV/c)^2. The corresponding differential yield curve is shown in Fig. 10(B). In both representations the η production is clearly seen.

Measurements of the η yield are rendered difficult by the proximity to the ρ-meson yields. At low energies and moderate $|t|$ values, the separation from the ρ signal is clear. At 9 GeV it is still possible to distinguish

η yields in the region of $t = -0.7$ (GeV/c)^2. At higher energies, the separation of the η step from the rising ρ yield was ambiguous and we do not include these measurements.

Figure 11 shows the measured η cross section $s^2\, d\sigma/dt$ as a function of t for primary photon energies of 5.5, 6.0, 6.5, and 9 GeV. For comparison, the measured π^0 cross-section curve at 6 GeV is shown as the dashed line. The difference between the η and π^0 angular distributions is very striking. Whereas the π^0 cross section shows a dip around $t = -0.5$ (GeV/c)^2 followed by a secondary maximum, the t dependence of the η cross section for t between -0.3 and -1.1 (GeV/c)^2 shows no structure. For the range of energies covered in this experiment, the energy dependence of the cross section is consistent with s^{-2}.

FIG. 11. $s^2\, d\sigma/dt$ in μb GeV^2 plotted versus t for the reaction $\gamma + p \rightarrow \eta + p$ for photon energies between 5.5 and 9 GeV. The dotted line shows the π^0 cross section at 6 GeV for comparison purposes.
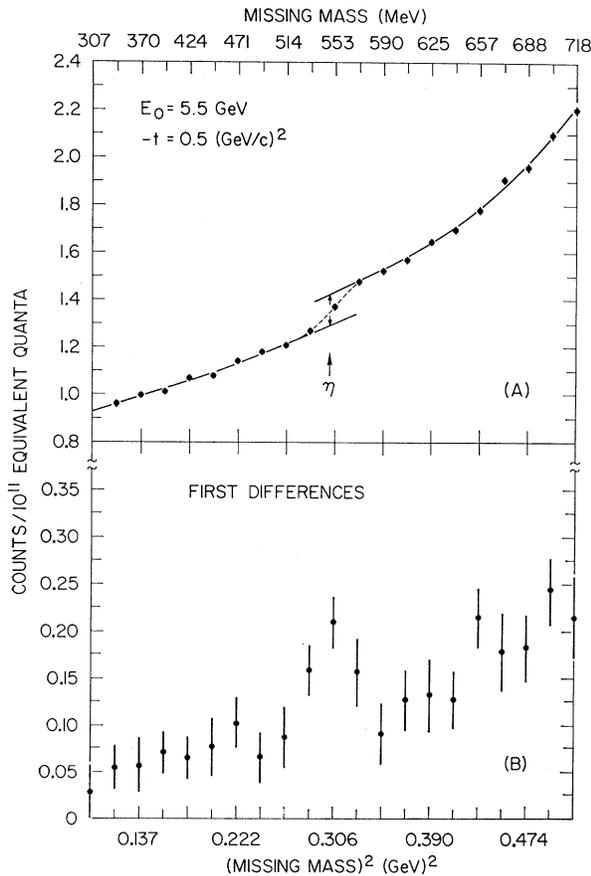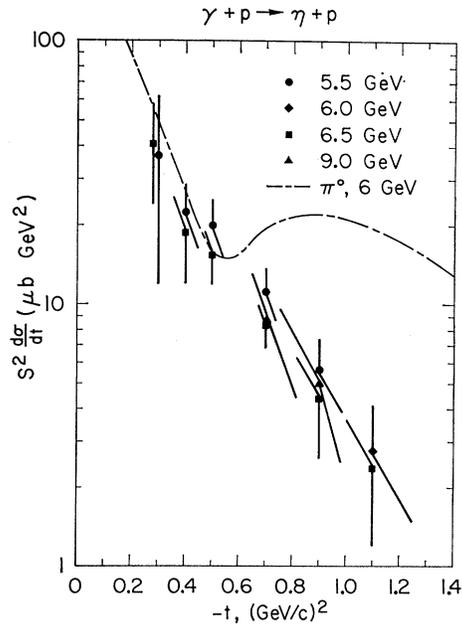

FIG. 10. (A) Measured proton yield in the vicinity of the η step is plotted versus missing mass squared for an end-point bremsstrahlung energy of 5.5 GeV and $t = -0.5$ (GeV/c)^2. The ordinate is counts per hodoscope element per 10^{11} E.Q. (B) Differential curve derived from the integral yield curve in (A). Plotted is the difference, in counts per 10^{11} E.Q., between once-removed yield points versus missing mass squared.

[31] A. Dar *et al.*, Phys. Rev. Letters **20**, 1261 (1968).

Figure 12 shows a comparison of our data (assuming s^{-2}) with the CEA data[6] taken at a primary photon energy of 4 GeV. Plotted is $s^2\, d\sigma/dt$ versus t. The agreement is moderate, our results appearing somewhat systematically higher than the CEA results. This might arise either from an energy dependence other than s^{-2} or from experimental biases. The integral yield method we used is less likely to result in experimental bias than the CEA coincident-photon measurements which involved a variety of cuts on the data to extract the cross sections.

The photoproduction of η's at forward angles should have a large contribution from Reggeized ρ exchange. This would then lead to a dip in the cross section in the vicinity of $t = -0.5$ (GeV/c)^2 where the ρ trajectory

passes through 0. The absence of such a dip in the data is puzzling. The class of theories[32] which explain the dip in π^0 photoproduction and $\pi^- p$ charge exchange as due to interference terms between the pole terms and the cut terms could lead to a natural explanation of both the neutral π and η photoproduction results.

By assuming only ρ exchange, Dar and Weisskopf[33] relate the η cross section to the reaction $\gamma + p \rightarrow \omega + n$. Using the data taken at 3.25 (GeV/c), they achieved reasonable agreement with this experiment using $\gamma_\omega^2/4\pi$ $= 2.9$. Gorczyca and Hayashi[34] include ω and B exchange
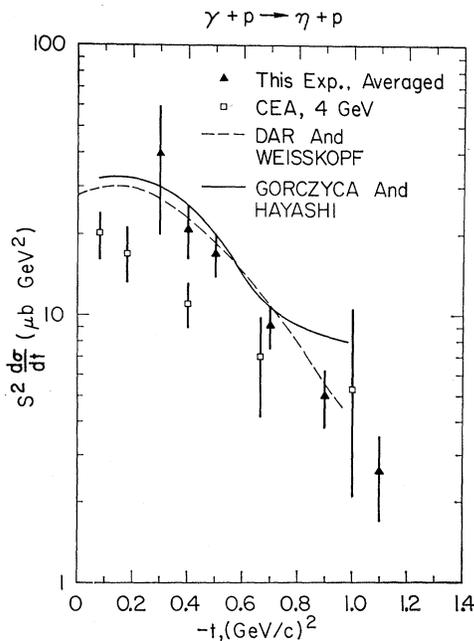
$$\gamma + p \longrightarrow \eta + p$$

FIG. 12. Results of this experiment compared with the results of an experiment at CEA at 4 GeV. Plotted is $s^2\, d\sigma/dt$ in μb GeV^2 versus t. The dashed line is the cross section predicted by Dar and Weisskopf using vector dominance and assuming only ρ exchange. The solid line is a prediction by Gorczyca and Hayashi based on vector dominance but allowing ω and B exchange in addition to ρ exchange. The two predictions assumed different values for the coupling constant $g_{\omega\gamma}$.

as well. They also achieve reasonable agreement with the data. Both predictions are plotted in Fig. 12

These models,[33,34] although giving reasonable predictions, do not clarify the basic underlying mechanisms involved in η production.

V. ρ-ω PRODUCTION

In the course of this experiment we obtained about 60 yield curves suitable for extracting ρ^0 cross sections.

Figure 13(A) shows a typical yield curve. Figure 13(B) is a plot of the first differences of the yields, and

[32] F. Henyey *et al.*, Phys. Rev. Letters **21**, 946 (1968).

[33] A. Dar and V. F. Weisskopf, Phys. Rev. Letters **20**, 762 (1968).

[34] B. Gorczyca and M. Hayashi, Institute of Theoretical Physics, Jagellonian University, Cracow, Poland Report (unpublished).
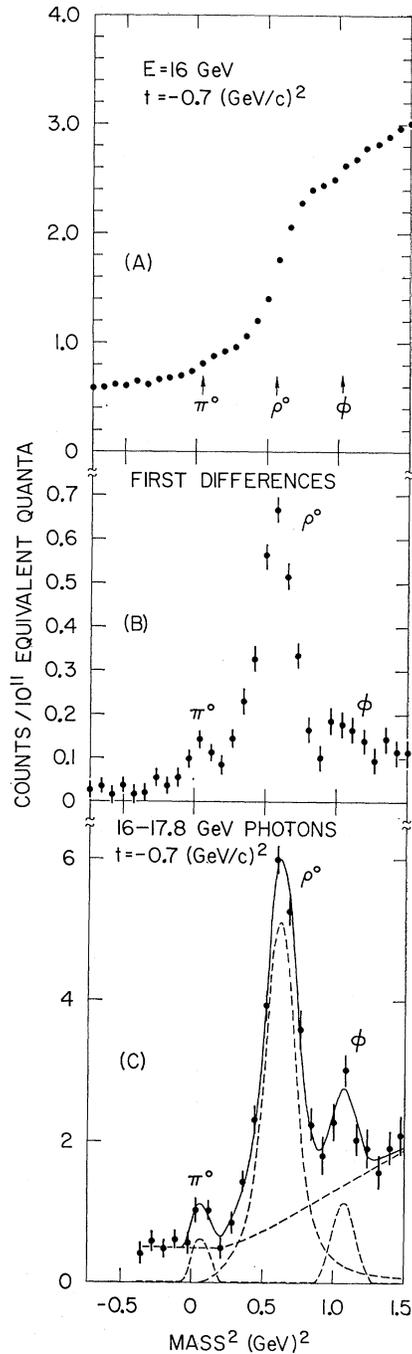
FIG. 13. (A) Measured proton yield per hodoscope element per 10^{11} E.Q. plotted versus missing mass squared for an end-point bremsstrahlung energy of 16 GeV and $t = -0.7$ (GeV/c)^2. The positions of the steps due to the onset of π^0, ρ, and ϕ production are indicated. (B) Differential yield curve obtained from the integral yield curve in (A). Plotted is the difference in counts between once-removed points per 10^{11} E.Q. The peaks due to π^0, ρ^0, and ϕ production are clearly seen. (C) Subtracted proton yield curve in counts per hodoscope counter per 10^{11} E.Q. for photons between 17.8 and 16 GeV and $t = -0.7$ (GeV/c)^2 plotted versus missing mass squared. This curve was obtained by subtracting the 16-GeV proton yield from the corresponding yield at 17.8-GeV end-point energy. The solid line through the data points represents a least-squares fit assuming π^0, ρ^0, and ϕ production in addition to nonresonant background. The breakdown of the yield into the separate contributions is shown as dashed lines.

has the distinctive ρ peak at around 765 MeV. Figure 13(C) shows a difference curve obtained by subtraction between two close end-point energies. All three curves contain essentially the same information. We had insufficient resolution to distinguish ω production clearly from neutral ρ production. For the purposes of analyzing the data we assumed that the ω cross sections were 10% of the ρ cross sections. This should be a good approximation since at high energies the nondiffractive part of the ω production is small and the ratio between ω and ρ should be given by $SU(3)$. This has been confirmed experimentally.[12]

It was hard to draw definitive conclusions as to the shape of the ρ decay spectrum. At high energies and low t values, the resolution of the apparatus became comparable to the width of the ρ. At low energies, although the resolution was very adequate, the background of multipion events under the ρ peak became large and produced some ambiguities in the interpretation. These ambiguities were most serious with respect to the shape and less serious with respect to the total cross section.

A large number of shapes and widths for the ρ meson were investigated and are listed below.

(a) A relativistically correct generalization of the simple Breit-Wigner form, as described by Jackson and Selleri.[35]

(b) A form suggested by Ross and Stodolsky[36] where the above shape is multiplied by the additional factor of $(m_\rho/m)^4$. Although this factor is disputed, at least one experiment indicates it may be a good description of the ρ shape.[8] Other powers of m_ρ/m were also tried.

(c) The Söding interference model.[37] Because our method integrates over the whole resonance, the interference term tends to cancel out, and the results are not significantly different from those for the Jackson shape.

(d) A simple nonrelativistic Breit-Wigner shape.

The background from nonresonant multipion production was estimated with a polynomial, which was kept to as few terms as possible consistent with a reasonable fit. With different assumed ρ shapes, the fitting program divided the observed yield into background and ρ signal differently. In general, cross sections obtained with the different models disagreed by 5–10%, with the Jackson shape giving values about 7% systematically higher than the Ross-Stodolsky shape. Our data did not significantly prefer any one shape. The Jackson shape tended to give better fits at high energies and high t values. The Ross-Stodolsky shape gave better fits at low t values and low energies, and gave poor fits at high energies and high t values.

Various experiments have measured ρ widths anywhere between 90 and 160 MeV and masses between 720 and 780 MeV.[7–10] Both these parameters were at first treated in this experiment as unknowns to be determined at each energy and momentum transfer. There was no observable dependence of the ρ mass on s or t. The best-fit mass value depended, of course, on the shape used. The Jackson form led to a mass of 765 ± 20 MeV, in agreement with the results of McClellan *et al.*[9] The Ross-Stodolsky form gave a value 10–20 MeV higher. The large ρ mass shift sometimes reported to be observed in photoproduction experiments[7,8,10] was not observed in this experiment. For each yield curve, a best ρ width was determined by stepping the input ρ width in 15 MeV increments between 80 and 170 MeV, simultaneously adjusting the background polynomial to give a best fit to the data. The error was taken to correspond to the point where the χ^2 probability had fallen to half of its best value. This criterion gave typical errors of ± 30 MeV. This large error arose because changes in the background polynomial could accommodate changes in the trial ρ width. In general, the preferred width was relatively independent of the ρ shape chosen. As with the mass, there was no systematic dependence of width on s or t. Including possible systematics, a best width of 127 ± 25 MeV was obtained.

All subsequent cross-section fitting, at all energies and momentum transfers, was made with the Jackson shape (a) for the ρ with a width of 125 MeV and a mass of 765 MeV plus a 10% ω contribution. The variations of the derived ρ cross sections with assumed ρ widths were, on the average, 5% for a 10-MeV change in width. For each yield curve, the sensitivity of cross section to width and the uncertainty in the width were used to estimate errors. In general, the presence of nonresonant background was the cause of the above systematic uncertainties and the assigned systematic error was approximately equal to ± 30% of the nonresonant background. The nonresonant background was largest at low energies where processes other than diffractive are still important, and at high t values where again the diffractive contributions are not so dominant.

Our results, when analyzed consistently, showed high internal consistency. This internal consistency does not necessarily correlate with real precision in the cross-section determinations, and our quoted results may therefore be systematically distorted to run either high or low through our error bars.

Figure 14 shows a comparison of our data in the energy range 5.5–6.5 GeV with a fit to the DESY data[38] at nearby energies. Also included on the figure are the results of McClellan *et al.*[9] at 6 GeV. The agreement between the three sets of data is good.

Both from the vector-dominance model and on more

---

[35] J. D. Jackson, Nuovo Cimento **34**, 1644 (1964); F. Selleri, Phys. Letters **3**, 76 (1962).
[36] M. Ross and L. Stodolsky, Phys. Rev. **149**, 1172 (1966).
[37] P. Söding, Phys. Letters **19**, 702 (1966).

[38] Aachen-Berlin-Bonn-Hamburg-Heidelberg-München Collaboration, Phys. Letters **27B**, 54 (1968).

general grounds,[39] we should expect for $|t|$ values where diffractive scattering is dominant that the photoproduction of ρ^0 mesons will be related by a constant of proportionality C_ρ to elastic ρ^0-p scattering:

$$\frac{d\sigma}{dt}(\gamma\rho^0) = C_\rho \frac{d\sigma(\rho^0 p)}{dt}. \quad (5.1)$$

Substituting the quark-model prediction[11] from Eq. (1.2) into this relation, we obtain

$$\frac{d\sigma}{dt}(\gamma\rho^0) = C_\rho \left[\frac{1}{2}\left(\frac{d\sigma}{dt}(\pi^+ p)\right)^{1/2} + \frac{1}{2}\left(\frac{d\sigma}{dt}(\pi^- p)\right)^{1/2}\right]^2. \quad (5.2)$$

Figure 15 shows a comparison between our results and these theoretical predictions using the elastic pion scattering data of Foley et al.[40] with C_ρ as our only adjustable parameter. The theoretical prediction is plotted as the solid lines together with the experimental data points. The agreement is remarkably good over the t range from -0.2 to -0.7 (GeV/c)^2 at 6.5 GeV and over the entire t range at higher energies.

It does not seem possible that this agreement with theory is fortuitous, and we therefore believe the error is small in extrapolating our data to $t=0$ using the above-predicted shape, at least at the higher energies. Table II gives values of $(d\sigma/dt)_{t=0}$ and of σ_T obtained from this shape with a single best value of C_ρ. We also give values of $(d\sigma/dt)_{t=0}$ and σ_T, where we assume the shape is represented by the above formula over the $|t|$-value range 0.1–0.7 (GeV/c)^2 but permit C_ρ to vary with energy. The forward cross section analyzed either way drops from an average value of 130–140 μb/(GeV/c)^2 around 6 GeV to an average value 102 μb/(GeV/c)^2 around 17 GeV.

McClellan et al.[9] report the cross section at $t=0$ as ~ 140 μb/(GeV/c)^2 in the range 5–10 GeV. Within errors this is consistent with our values. However, their values show less of a trend to decrease with energy over this range. We note that their cross-section determinations, like ours, are dependent on the specific shape and background assumptions. Their measurements, based on observation of the final two-pion state, have less severe background problems than ours. However, our statistical precision is much higher and our integral yield measurements are automatically summed over the ρ mass spectrum with nearly the appropriate weights. We are thus less sensitive to exact spectral shapes than are methods based on taking weighted samples in the neighborhood of the ρ decay peak.

---

[39] See, for instance, S. D. Drell and J. S. Trefil, Phys. Rev. Letters **16**, 552 (1966), in which the angular dependence of ρ^0-meson photoproduction on complex nuclei is obtained without any explicit reference to the assumptions of a strict vector-dominance theory.

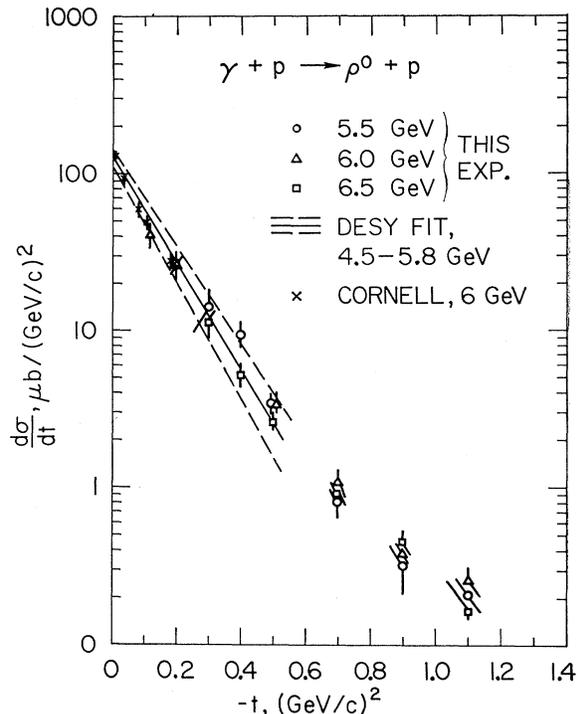[40] K. J. Foley et al., Phys. Rev. Letters **11**, 425 (1963).]

FIG. 14. $d\sigma/dt$ in μb/(GeV/c)^2 plotted versus t for the reaction $\gamma+p \to \rho^0+p$ for photon energies between 5.5 and 6.5 GeV. The solid line is a least-squares fit by the DESY bubble-chamber group to their data for photon energies between 4.5 and 5.8 GeV. Acceptable limits to their fits are indicated by the dashed lines. The results of a measurement at Cornell (Ref. 9) for an end-point energy of 6 GeV are also shown.

We can use the vector-dominance relation

$$\left.\frac{d\sigma}{dt}\right|_{t=0} = \frac{1}{4}\alpha \frac{4\pi}{\gamma_\rho^2} \frac{\sigma_T^2(\rho^0 p)}{16\pi} \quad (5.3)$$

to relate our mean value of C_ρ to $\gamma_\rho^2/4\pi$, the usual vector-dominance factor. The result is $\gamma_\rho^2/4\pi = 0.61$.

TABLE II. Forward differential and total ρ cross sections obtained from fits to our data calculated both with a best-fit constant C_ρ from Eq. (5.3) and with an energy-dependent C_ρ best-fitted at each energy.

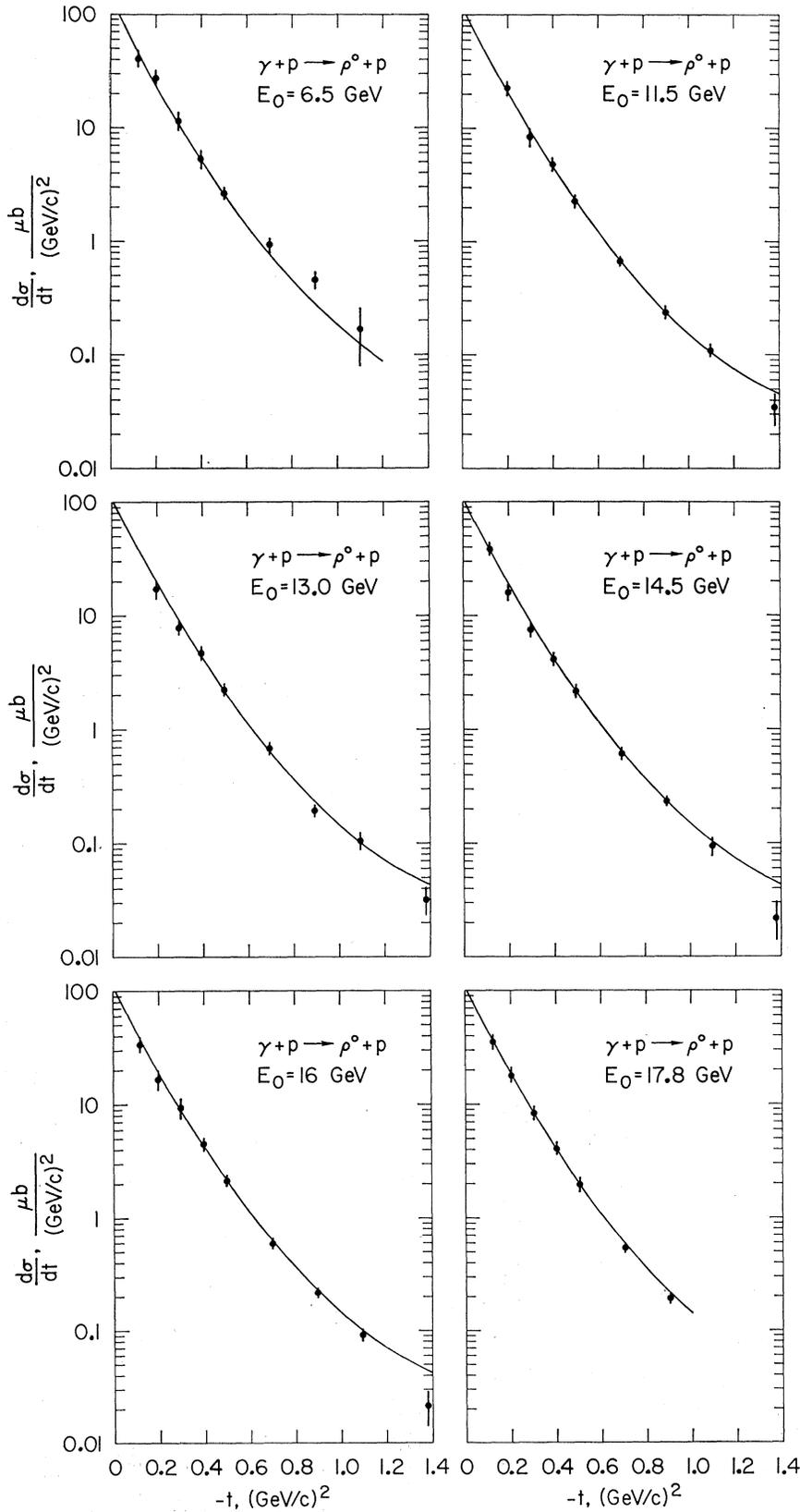| E_0 (GeV)	Constant C_ρ		Energy-dependent C_ρ		
	$d\sigma/dt$ ($t=0$) [μb/(GeV/c)^2]	σ_T (μb)	$d\sigma/dt$ ($t=0$) [μb/(GeV/c)^2]	σ_T (μb)	% error
17.8	104.6	12.39	100.5	11.89	±5
16.9	105.3	12.47	105.3	12.47	±6
16.0	105.9	12.55	103.3	12.24	±6
15.25	106.7	12.65	106.6	12.54	±6
14.5	107.6	12.74	101.2	11.98	±6
13.75	108.8	12.87	109.5	12.95	±5
13.0	110.1	13.04	108.7	12.86	±6
12.25	111.6	13.23	111.4	13.19	±6
11.5	113.4	13.44	113.4	13.44	±6
6.5	131.0	15.50	137.6	16.27	±10
6.0	133.3	15.79	151.9	18.0	±10
5.5	135.8	16.09	166.9	19.8	±12

Fig. 15. $d\sigma/dt$ in μb/$(\mathrm{GeV}/c)^2$ versus t for the reaction $\gamma+p \rightarrow \rho^0+p$ at incident photon energies from 6.5 to 17.8 GeV. The lines drawn through the data points are a best fit to the quark relation in Eq. (5.2). The one adjustable parameter C_ρ was set to a value of 2.98×10^{-3}.
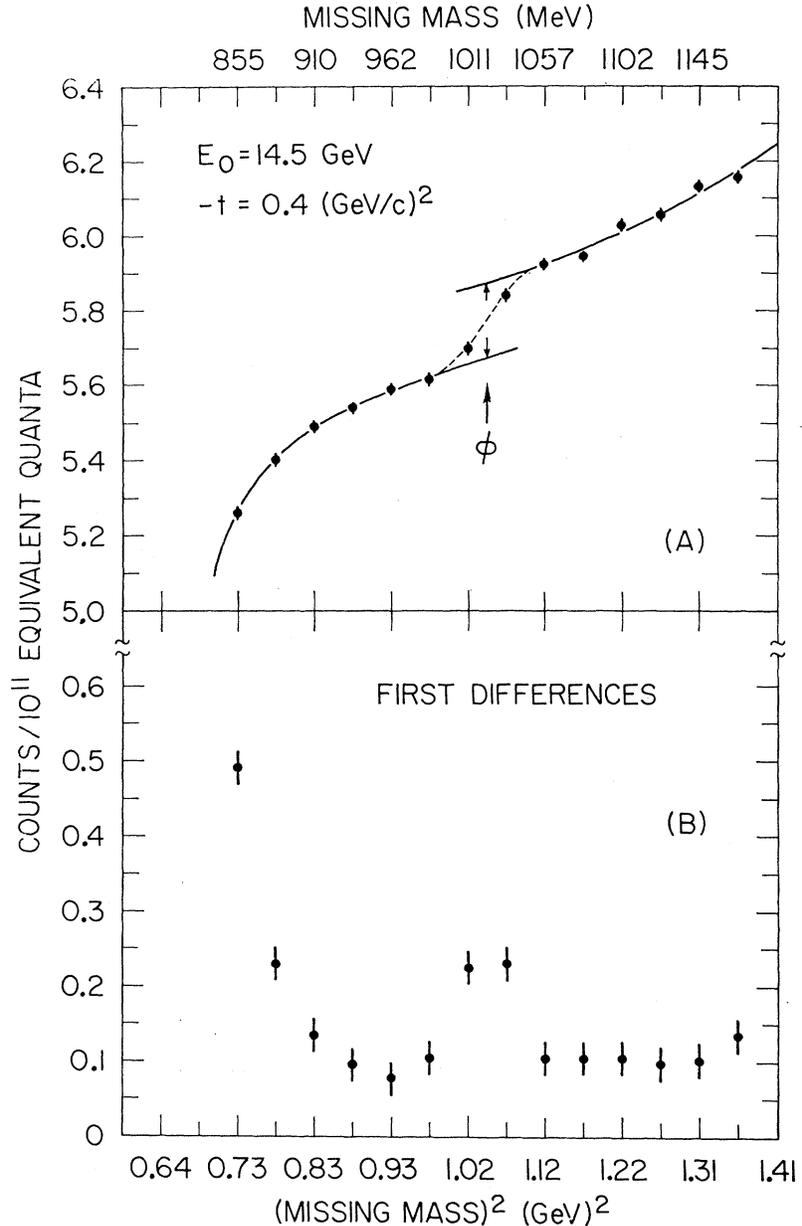
FIG. 16. (A) Measured proton yield in counts per hodoscope element per 10^{11} E.Q. plotted versus missing mass squared in the region around the ϕ step for an incident photon energy of 14.5 GeV and for $t=-0.4$ $(GeV/c)^2$. (B) Differential yield curve derived from the above integral curve. Plotted is the difference in counts between once-removed hodoscope elements per 10^{11} E.Q. versus missing mass squared.

If, instead, we use $\sigma_T=30$ mb at 9 GeV, from Bulos et al.[41] we obtain $\gamma_\rho^2/4\pi=0.7$. If we assume $\sigma_T=39$ mb at 6 GeV, from McClellan et al.[42] we get $\gamma_\rho^2/4\pi=1.09$. Thus a value of $\gamma_\rho^2/4\pi=0.45$ is not consistent with a vector-dominance theory relating the ρ^0 photoproduction cross section at $t=0$ of 120–130 μb/$(GeV/c)^2$, as measured in this and other experiments, to ρ-nucleon total cross sections in the range 30–40 mb.[8,41,42]

[41] F. Bulos et al., Phys. Rev. Letters **22**, 490 (1969); cf. also Asbury et al., ibid. **19**, 865 (1967).

[42] G. McClellan, Phys. Rev. Letters **22**, 377 (1969).

VI. ϕ PRODUCTION

The ϕ-meson production cross sections were considerably smaller than the ρ^0 cross sections. The proton yield from ϕ production comes in a region where the lower-energy components of the bremsstrahlung beam also produce a very large yield of protons associated with ρ production and nonresonant background. As with the ρ, the single-to-noise ratio improved at high energies where the diffractive processes dominated, and measurements at low $|t|$ values were difficult because of the poor angular resolution caused by the multiple Coulomb scattering in the target. Figure 16(A) and 16(B) show
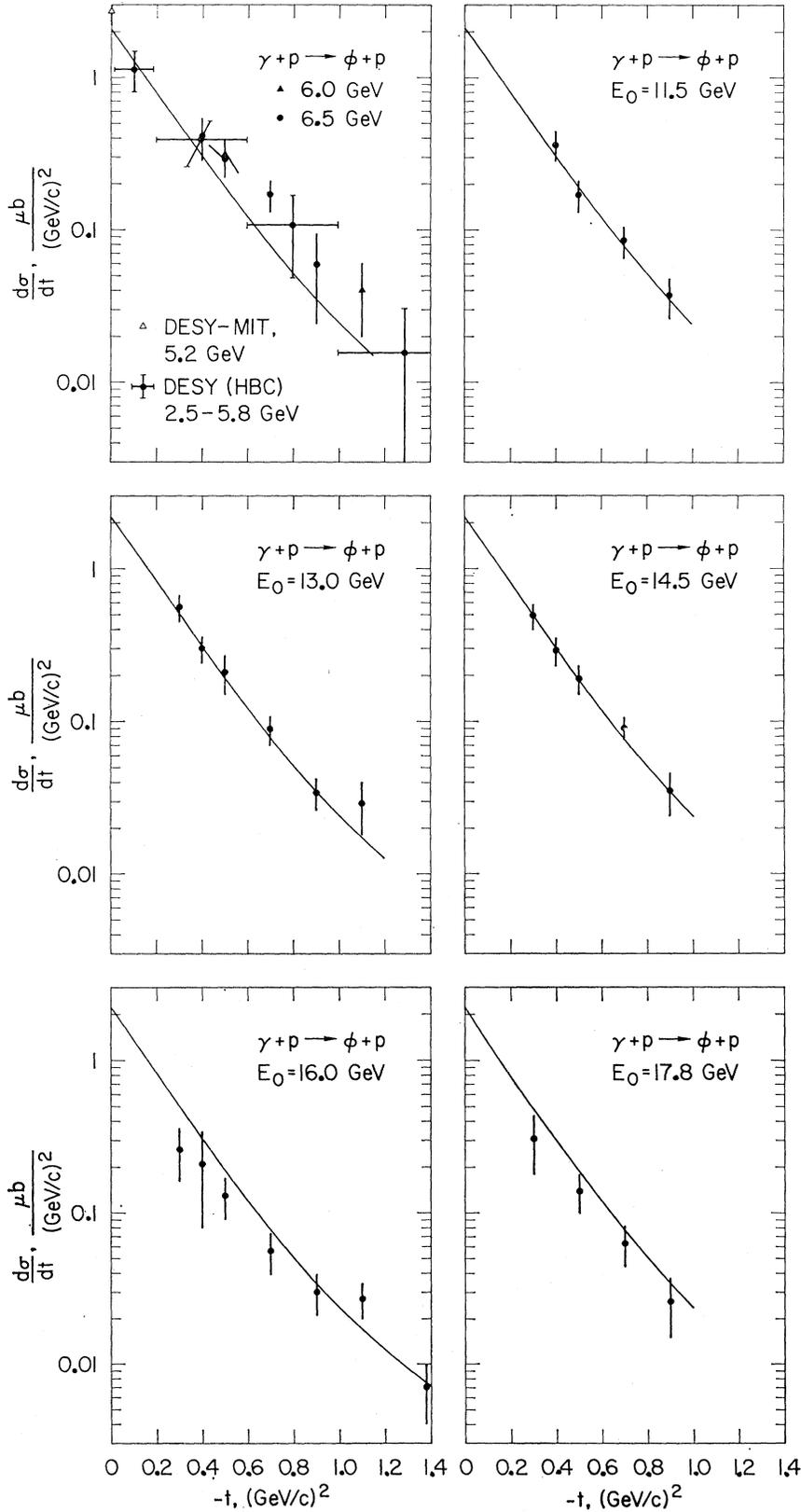
FIG. 17. $d\sigma/dt$ in μb/$(GeV/c)^2$ versus t for the reaction $\gamma + p \rightarrow \phi + p$ at incident photon energies between 6 and 17.8 GeV. At 6 GeV we have included the DESY bubble-chamber results (Ref. |8) and the result at $t=0$ of Asbury *et al.* (Ref. 8). The solid line is a best fit to the quark relations (6.1) and (6.2) with the one adjustable parameter C_ϕ set equal to 18.6 $\times 10^{-5}$.

typical integral and first-difference yield plots in the region of the ϕ. While the small decay width of the ϕ gave a sharp and distinctive threshold in the yield curve, very good statistical precision was necessary to distinguish the ϕ production from background processes underneath the ϕ step. We analyzed the ϕ yield curves assuming relatively smooth backgrounds and made conservative error assignments on the basis of a detailed statistical analysis. A typical yield curve consisted of 20 points, each with a standard deviation of $\pm 0.3\%$, in the mass range 950–1150 MeV, and with a ϕ-step change of 3% superimposed on the background. Under these conditions, we typically assigned to the step height an error of $\sqrt{2}$ times the absolute standard deviation for one yield point, or a relative error on the final quoted ϕ cross section of about $\pm 15\%$.

Figure 17 shows our results for different energies plotted versus t. We have included for comparison with our 6.5-GeV data the DESY point of Asbury *et al.*[8] at $t\simeq 0$, and at higher $|t|$ values the results of the DESY bubble-chamber experiment.[8] Agreement is satisfactory.

The solid line represents the theoretical predictions based on the assumptions of the quark model.[11] We assumed[43] that

$$\frac{d\sigma}{dt}(\gamma\phi) = C_\phi \frac{d\sigma}{dt}(\phi p), \tag{6.1}$$

$$\frac{d\sigma}{dt}(\phi p) = \left[\left(\frac{d\sigma}{dt}(K^+ p)\right)^{1/2} + \left(\frac{d\sigma}{dt}(K^- p)\right)^{1/2} \right.$$
$$\left. -\left(\frac{d\sigma}{dt}(\pi^- p)\right)^{1/2}\right]^2. \tag{6.2}$$

The $K^+ p$ and $K^- p$ cross sections were taken from the experiment of Foley *et al.*[44] The t dependence is well represented by the quark relation. There is an indication in the data of a decrease in C_ϕ and a corresponding decrease in the total ϕ cross section with increasing photon energies. The fit to the data with varying C_ϕ gave, at 6-GeV incident photon energies, a forward cross section of 3.2 ± 0.4 μb/(GeV/c)^2 and a total ϕ cross section of 0.71 ± 0.08 μb. Averaged over photon energies between 11.5 and 17.8 GeV, the forward cross section was 2.1 ± 0.2 μb/(GeV/c)^2 and the total cross section was 0.45 ± 0.04 μb. A change in C_ϕ with energy is in some disagreement with the quark model. However, since the connection equation (6.2) between the theoretical ϕp elastic cross sections and the physically observed strong-interaction cross sections involved large subtrac-

tions, this apparent discrepancy does not seem too significant.

Our value for $\gamma_\phi^2/4\pi$ as derived from the average value of C_ϕ is 9.8. Within the uncertainties in the present values of $\gamma_\phi^2/4\pi$, this is in reasonable agreement with the theoretical expectation[45] that the ratio $\gamma_\rho^2 : \gamma_\phi^2$ should be $1.33 : 9$.

VII. OTHER MESON PRODUCTION

The $X^0(958)$ meson is expected to be produced with cross sections comparable to those of the η meson.[33] However, the X^0 meson was not clearly resolved from the ρ meson. Upper limits to the cross sections in the 6-GeV range gave values less than two or three times the observed η cross sections, in no contradiction to the theoretical expectation.
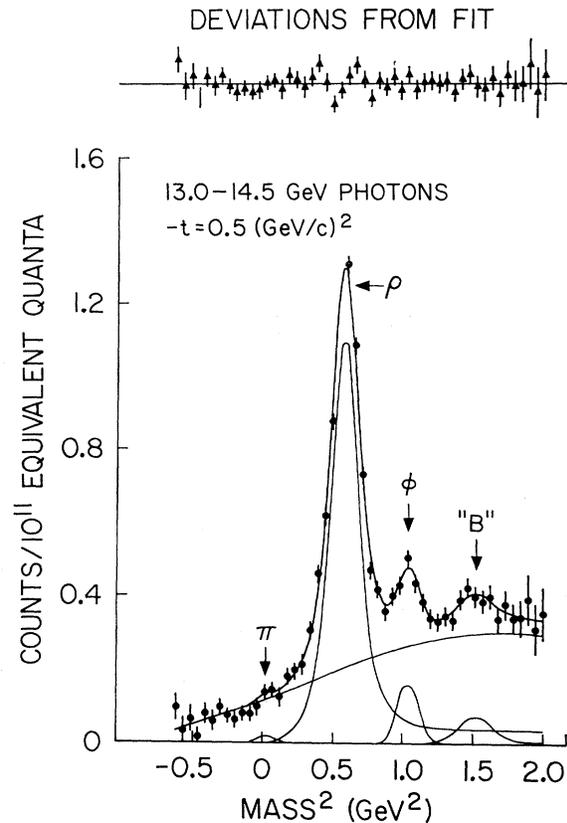

Fig. 18. Subtracted proton yield per hodoscope element per 10^{11} E.Q. plotted versus missing mass squared for photons between 14.5 and 13 GeV. The peaks due to ρ^0 and ϕ production can be seen. In addition, the curve shows a particle with mass of about 1250 MeV ("B") being produced with roughly the same cross section as the ϕ. The solid curve is a least-squares fit to the data assuming π^0, ρ^0, ϕ, and the "B" meson in addition to a smoothly varying amount of background. The relative contributions are indicated in the figure.

---

[43] Relation (6.2) is not the relation usually quoted in the literature (cf. Ref. 11). The generally quoted relation is $\sigma_T(\phi p) = 2\sigma_T(K^+ p) + \sigma_T(\pi^- p) - 2\sigma_T(\pi^+ p)$. This relation makes use of an additional assumption based on the Pomeranchuk theorem to eliminate the use of $K^- p$ cross sections.

[44] K. J. Foley *et al.*, Phys. Rev. Letters **11**, 503 (1963); **15**, 45 (1965).

[45] R. J. Oakes and J. J. Sakurai, Phys. Rev. Letters **19**, 1266 (1967). This is now the most generally accepted derivation of this ratio. References to the many earlier papers on this ratio can be found in the above reference.
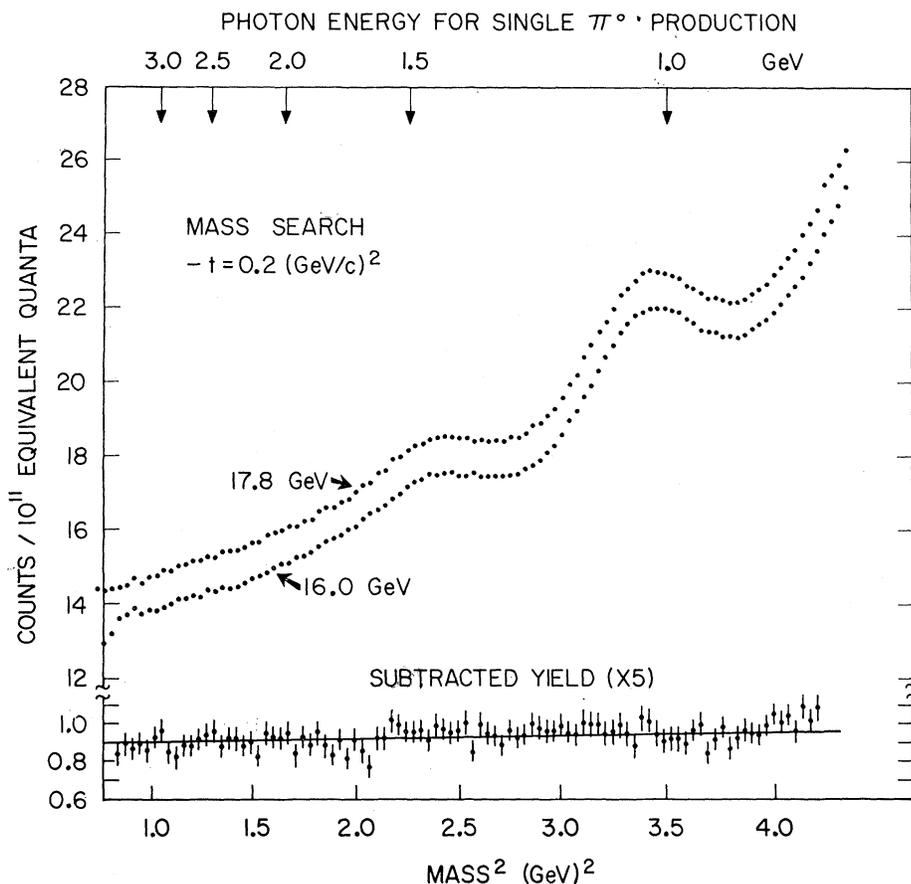
PHOTON ENERGY FOR SINGLE π^0 ' PRODUCTION

FIG. 19. Shown are the results of a mass search in the region of missing mass squared of 1.5–4 GeV² for $t = -0.2$ (GeV/c)². Plotted is the proton yield per hodoscope element per 10^{11} E.Q. as a function of missing mass squared for end-point energies of the bremsstrahlung spectrum of 17.8 and 16 GeV, respectively. The structure seen in these curves was due to low-energy single π^0 production. The upper scale shows the photon energy responsible for single π^0 production. The prominent bumps are associated with the third and fourth resonances. The subtraction between the two properly normalized yield curves then corresponds to reactions initiated by photons between 17.8 and 16 GeV. The result of this subtraction is shown in the figure on an expanded scale. The solid line is a least-squares fit of a straight line to the data.

At high energies, we saw indications for the production of a broad resonance centered at 1240±20 MeV with a width of around 100 MeV. We covered an appropriate range of mass values for measuring the production of a 1240-MeV mass particle on about 15 sweeps. All of the sweeps taken at 13 and 14.5 GeV in the range of $t = -0.3$ to $t = -0.7$ (GeV/c)² gave evidence for such a resonance. Figure 18 shows a representative mass sweep obtained by subtracting the yields taken at 14.5 and 13 GeV for $t = -0.5$ (GeV/c)². At higher energies this mass scale was compressed, and at lower energies the backgrounds increased, making the signals less clear. Qualitatively, this meson (or possibly mesons) was produced with cross sections of the same order as the ϕ in the energy range 13.0–14.5 GeV and the $|t|$-value range 0.3–0.7 (GeV/c)². We tentatively identify this signal with the B meson whose quantum numbers $J^{PC} = 1^{+-}$ would permit it to be quasidiffractively produced.[46] It is possible that this particle could be an as-yet-undiscovered vector meson.

We have also searched for the production of resonances with masses between 1.3 and 2 GeV at $t = -0.2$ (GeV/c)² and ~17-GeV photon energy. The low $|t|$ value and high energy should be especially suitable for singling out states that could be diffractively produced. In particular, we might have expected to observe any new vector mesons in this mass range such as the $J^{PC} = 1^{--}$ state on the "daughter" trajectory of the ρ trajectory.

A single integral yield curve shows structure arising from both the high-energy photoproduction of high-mass states and from lower-energy photon production of single-pion or other low-mass states. Therefore for this survey we used a subtraction of two sweeps taken

TABLE III. Upper limits to cross sections in the missing-mass search at 16.9-GeV average photon energy at $t = -0.2$ (GeV/c)² for the production of particles with widths 100 and 200 MeV.

| | 100-MeV width | | 200-MeV width | |
| | Upper limit for $\dfrac{d\sigma}{dt}$ | Upper limit for $\dfrac{d\sigma}{dt} \Big/ \dfrac{d\sigma}{dt}(\rho)$ | Upper limit for $\dfrac{d\sigma}{dt}$ | Upper limit for $\dfrac{d\sigma}{dt} \Big/ \dfrac{d\sigma}{dt}(\rho)$ |
Mass (MeV)	[μb/(GeV/c)²]		[μb/(GeV/c)²]	
1300	0.49	0.022	0.69	0.031
1450	0.54	0.024	0.76	0.034
1600	0.61	0.028	0.87	0.039
1800	0.71	0.032	1.00	0.045

[46] D. R. O. Morrison, Phys. Letters 22, 528 (1966).

at 17.8- and 16-GeV peak energies. Figure 19 shows both the unsubtracted and subtracted yields. The integral yield curves represent on the order of 2×10^7 counts each. Any produced particle would show up as a peak in the subtracted yield curve. No such peak can be seen in the data. To determine the statistical significance level of this mass search, we have made an analysis of the data with the following method. A straight line (two parameters) was fitted to the subtracted yield curve. This fit, although expected to be poor in the region of masses just above the ϕ, gave a good representation of the data with a χ^2 of 82 for 93 degrees of freedom. We then searched the subtracted yield curve for any significant peaks superimposed on this smooth linear fit. This was done by computing the ratio

$$\sum_i W_i(n,a)T_i / (\sum_i W_i^2 \sigma_i^2)^{1/2}, \qquad (7.1)$$

where T_i is the difference between the measured yield in mass bin i and the straight-line fit, W_i is a Gaussian "weight function" centered in bin n with a full width at half-maximum of a, and σ_i is the error assigned to the measured point in bin i. The above quantity was then centered on each bin and computed for several choices of a between 50 and 250 MeV. For none of the large number of possible combinations was the above ratio larger than 3.0. We set our level of significance as 5 for this ratio. The resulting upper limits to the cross sections for widths of 100 and 200 MeV are given in Table III.

We checked for internal consistency by searching the data for "negative" or nonphysical inverted peaks. In this case the ratio was never larger than 2.5.

At the energy of 16.9 GeV, the minimum four-momentum transfer squared to the nucleon for the

production of a meson as massive as 2 GeV is -0.014 $(GeV/c)^2$ and is small compared with the value of $t = -0.2$ $(GeV/c)^2$ at which the measurement was made. Therefore, there should be no inhibition on the production of a 2-GeV-mass meson from this cause. It is possible that a high-mass vector meson might escape observation in production experiments if it decayed into ω mesons and π^0 mesons which would give final states containing two neutral pions. Since this is a missing-mass experiment, our observations are completely independent of the decay modes open to the particle. We conclude from Table III that at a 90% confidence level no particle with a cross section larger than about 5% of the ρ^0 cross section was produced in the mass region 1.3–2 GeV.